

Mechanical Weyl Modes in Topological Maxwell Lattices

D. Zeb Rocklin,¹ Bryan Gin-ge Chen,^{2,*} Martin Falk,³ Vincenzo Vitelli,² and T. C. Lubensky⁴

¹*Department of Physics, University of Michigan, 450 Church St. Ann Arbor, MI 48109, USA*

²*Instituut-Lorentz, Universiteit Leiden, 2300 RA Leiden, The Netherlands*

³*Department of Physics, Massachusetts Institute of Technology,
77 Massachusetts Avenue Cambridge, MA 02139-4307, USA*

⁴*Department of Physics and Astronomy, University of Pennsylvania, Philadelphia, PA 19104, USA*

(Dated: October 19, 2015)

Topological mechanical structures exhibit robust properties protected by topological invariants. In this letter, we study a family of deformed square lattices that display topologically protected zero-energy *bulk* modes analogous to the massless fermion modes of Weyl semimetals. Our findings apply to sufficiently complex lattices satisfying the Maxwell criterion of equal numbers of constraints and degrees of freedom. We demonstrate that such systems exhibit pairs of oppositely charged Weyl points, corresponding to zero-frequency bulk modes, that can appear at the origin of the Brillouin zone and move away to the zone edge (or return to the origin) where they annihilate. We prove that the existence of these Weyl points leads to a wavenumber-dependent count of topological mechanical states at free surfaces and domain walls.

PACS numbers: 62.20.D-, 03.65.Vf

Topological properties of the energy operator and associated functions in wavevector (momentum) space can determine important properties of physical systems¹⁻³. In quantum condensed matter systems, topological invariants guarantee the existence and robustness of electronic states at free surfaces and domain walls in polyacetylene^{4,5}, quantum Hall systems^{6,7} and topological insulators⁸⁻¹³ whose bulk electronic spectra are fully gapped (i.e. conduction and valence bands separated by a gap at all wavenumbers). More recently topological *phononic* and *photonic* states have been identified in suitably engineered classical materials as well,¹⁴⁻³¹ provided that the band structure of the corresponding wave-like excitations has nontrivial topology.

A special class of topological mechanical states occurs in *Maxwell lattices*, periodic structures in which the number of constraints equals the number of degrees of freedom in each unit cell³². In these mechanical frames, zero-energy modes and states of self stress (SSS) are the analogs of particles and holes in electronic topological materials¹⁵. A zero energy (frequency) mode is the linearization of a *mechanism*, a motion of the system in which no elastic components are stretched. States of self stress on the other hand guide the focusing of applied stress and can be exploited to selectively pattern buckling or failure¹⁷. Such mechanical states can be topologically protected in Maxwell lattices, such as the distorted kagome lattices of Ref. 15, in which no zero modes exist in the *bulk* phonon spectra (except those required by translational invariance at wavevector $\mathbf{k} = 0$). These lattices are the analog of a fully gapped electronic material. They are characterized by a topological polarization equal to a lattice vector \mathbf{R}_T that, along with a local polarization \mathbf{R}_L , determines the number of zero modes *localized* at free surfaces, interior domain walls separating different polarizations, and dislocations¹⁶. Because \mathbf{R}_T only changes upon closing the bulk phonon gap, these

modes are robust against disorder or imperfections.

In this paper we demonstrate how to create topologically protected zero modes and states of self-stress that extend throughout a sample. These enable the topological design of bulk soft deformation and material failure in a generic class of mechanical structures. As prototypes, we study the distorted square lattices of masses and springs shown in Fig. 1, and we show that they have phases that are mechanical analogs of Weyl semimetals³³⁻³⁷. In the latter materials, the valence and conduction bands touch at isolated points in the Brillouin zone (BZ), with the equivalent *phonon* dispersion for the mechanical lattice shown in Fig. 1(a). Points at which two or four bands touch are usually called Weyl and Dirac points, respectively. These points, which are essentially wavenumber vortices in 2D and hedgehogs in 3D, are characterized by a winding or Chern number^{1,3} and are topologically protected in that they can disappear only if points of opposite sign meet and annihilate or if symmetry-changing terms are introduced into the Hamiltonian. Weyl semi-metals exhibit lines of surface states at the Fermi level that terminate at the projection of the Weyl points onto the surface BZ. Weyl points have also been predicted³⁸ and observed³⁹ in photonic crystals and certain mechanical systems with pinning constraints that gap out translations²². In contrast, our examples consist of ordinary spring networks which suggest that the Weyl phenomenon is in fact generic to Maxwell lattices of sufficient complexity.

The full phase space of our distorted square lattices is six-dimensional; to keep our discussion simple, we fix three of the four sites in the unit cell and vary the equilibrium coordinates (x_2, y_2) of one of the sites. The resultant 2D phase diagram, shown in Fig. 1(b), exhibits a rich phenomenology: (1) a special point (SP) at the origin with two orthogonal lines of zero modes in its spectrum, (2) special lines (SLs) along which the spectrum

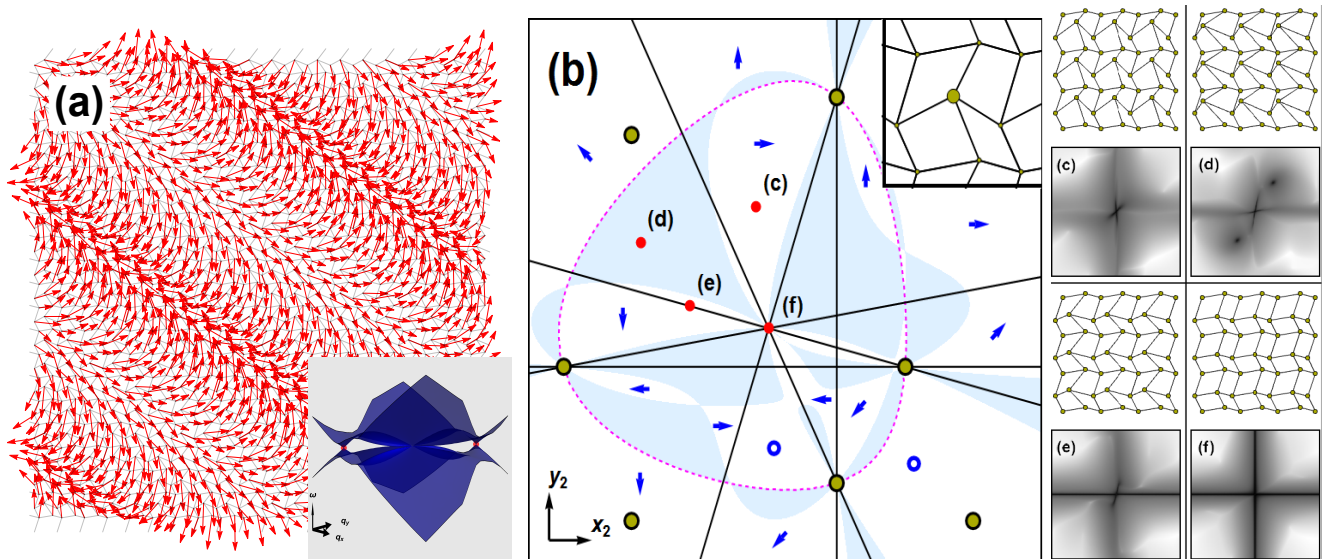


FIG. 1: (a) Deformed square lattices can have sinusoidal bulk zero modes (red arrows) corresponding to Weyl points where two bands touch in the phonon dispersion (inset). (b) The phase diagram of a deformed square lattice with the positions of three sites fixed and the position of the remaining site given by the position (x_2, y_2) , shown as an enlarged site in the inset. (c)-(f) Lattices (top) with phonon dispersions (bottom) with dark areas indicating low-energy modes in the Brillouin Zone. In (b), white areas such as (c) lack Weyl points and are marked with their a blue arrow indicating their topological polarization. Blue-shaded areas such as (d) correspond to Weyl lattices. Open boundaries between white and blue regions indicate where Weyl points emerge at $\mathbf{k} = (0, 0)$ while the pink dashed boundary indicate where they annihilate at $\mathbf{k} = (\pi, \pi)$. Lattices on the Special Lines, such as (e) lie between topological polarizations and possess lines of zero modes along $k_{x(y)} = 0$, while at the Special Point, (f), there are two zero modes along each of $k_{x(y)} = 0$.

exhibits a single line of zero modes, (3) finite regions in which the spectrum is fully gapped and characterized by topological polarizations \mathbf{R}_T , and (4) finite regions whose spectrum contains Weyl points. In (4), pairs of oppositely charged Weyl points corresponding to zero-frequency *bulk* modes appear at the origin of the BZ and

then move away to the zone edge or back to the origin where they annihilate. The existence of Weyl points has significant consequences for response at the boundaries, leading to a wavenumber-dependent count of boundary modes and SSS.

Lattices of periodically repeated unit cells in d dimensions with n sites (nodes) and n_B bonds per unit cell under periodic boundary conditions (PBCs) are characterized^{32,40} by an $n_B \times dn$ compatibility matrix $\mathbf{C}(\mathbf{k})$ for each wavevector \mathbf{k} in the BZ relating the dn -dimensional vector $\mathbf{u}(\mathbf{k})$ of site displacements to the n_B -dimensional vector $\mathbf{e}(\mathbf{k})$ of bond extensions via $\mathbf{C}(\mathbf{k})\mathbf{u} = \mathbf{e}(\mathbf{k})$ and by the $dn \times n_B$ equilibrium matrix $\mathbf{Q}(\mathbf{k}) = \mathbf{C}^\dagger(\mathbf{k})$ relating forces $\mathbf{f}(\mathbf{k})$ to bond tensions $\mathbf{t}(\mathbf{k})$ via $\mathbf{Q}(\mathbf{k})\mathbf{t}(\mathbf{k}) = \mathbf{f}(\mathbf{k})$. The dynamical matrix (for systems with unit masses and spring constants) is $\mathbf{D} = \mathbf{Q}(\mathbf{k})\mathbf{C}(\mathbf{k})$. Vectors $\mathbf{u}(\mathbf{k})$ in the null space of $\mathbf{C}(\mathbf{k})$ do not stretch bonds and, therefore, correspond to zero modes. Vectors $\mathbf{t}(\mathbf{k})$ in the null space of $\mathbf{Q}(\mathbf{k})$ describe states with tensions but without net forces and thus correspond to SSSs⁴¹. The number of zero modes $n_0(\mathbf{k})$ and SSSs $n_s(\mathbf{k})$ at each \mathbf{k} are related by the Calladine-

Maxwell index theorem⁴¹

$$\nu(\mathbf{k}) \equiv n_0(\mathbf{k}) - n_s(\mathbf{k}) = dn - n_B. \quad (1)$$

Lattices, like the square and kagome lattices in two dimensions, are *Maxwell lattices* that have the special property that $n_B = 2n = dn$ and, as a result, $n_0(\mathbf{k}) = n_s(\mathbf{k})$ for every \mathbf{k} . This relation states that for every \mathbf{k} there is one zero mode for each SSS and vice versa. Thus in a gapped system, there are no SSSs for any $\mathbf{k} \neq 0$, and at $\mathbf{k} = 0$, translational invariance requires $n_0(\mathbf{k}) \geq d$ and thus $n_s(\mathbf{k}) \geq d$. A Weyl point by definition is a \mathbf{k} at which there is a zero mode, and there is necessarily an SSS that goes with it. The lines of zero modes occurring along the SLs in the phase diagram also have associated lines of self-stress in real space.

We now turn to zero modes on free surfaces. Cutting a lattice under PBCs along a direction perpendicular to one of its reciprocal lattice vectors \mathbf{G} creates a finite-width

strip with two free surfaces aligned along the “parallel” direction perpendicular to \mathbf{G} . The cut removes Δn_B bonds and Δn sites for each unit cell along its length or equivalently for each wavenumber $-\pi/a_{\parallel} < q < \pi/a_{\parallel}$ along the cut, where a_{\parallel} is the length of the surface cell. The index theorem relating the total number of zero modes $N_0(q, \mathbf{G})$ to the total number of SSSs $N_s(q, \mathbf{G})$ at each q is

$$N_0(q, \mathbf{G}) - N_s(q, \mathbf{G}) = -d\Delta n + \Delta n_B. \quad (2)$$

Bulk modes in the spectrum are described by the same $\mathbf{C}(\mathbf{k})$ as the uncut sample but with a different set of quantized wavenumbers p parallel to \mathbf{G} . If a bulk mode is gapped in the periodic spectrum, it remains gapped in the strip without an associated state of self-stress. Thus if the bulk modes are gapped at a given q under PBCs, their contribution to the right-hand side of Eq. (2) will be zero, implying that only surface modes contribute to Eq. (2). In addition, cutting the sample will not introduce additional SSSs. The result is that Eq. (2) becomes an equation for the total number of zero surface modes on both surfaces:

$$n_0^{ST}(q, \mathbf{G}) = \Delta n_B - d\Delta n. \quad (3)$$

This is a global relation that applies to every q in the surface BZ at which the bulk spectrum is gapped.

In the bulk, our lattice is naturally described by a symmetric unit cell as depicted in Fig. 2(a). We associate with each lattice site a “charge” +2 and with the center of each bond a charge -1^{15} . The total dipole moment of this cell is zero. The number of zero modes for a surface perpendicular to \mathbf{G} can be calculated from the compatibility matrix $\mathbf{C}(\mathbf{k}, \mathbf{G}) \equiv \mathbf{C}(q, p, \mathbf{G})$ of another unit cell, one that is compatible with the surface \mathbf{G} (Fig. 2(b)). Its components are related to those of the compatibility matrix, $\tilde{\mathbf{C}}(\mathbf{k})$, of the symmetric unit cell via $C_{\beta, \sigma i} = e^{i\mathbf{k} \cdot \Delta \mathbf{r}_{\beta}} \tilde{C}_{\beta, \sigma i} e^{-i\mathbf{k} \cdot \Delta \mathbf{r}_{\sigma}}$, where $\beta = 1, \dots, n_B$ labels bonds, $\sigma = 1, \dots, n$ labels sites, and $i = x, y$ and $\Delta \mathbf{r}_{\beta}$ and $\Delta \mathbf{r}_{\sigma}$ are, respectively, the displacements of bond β and site σ necessary to convert the symmetric unit cell to the surface-compatible one. Both \mathbf{r}_{β} and \mathbf{r}_{σ} are necessarily Bravais lattice vectors. Thus,

$$\det \mathbf{C}(\mathbf{k}, \mathbf{G}) = \exp(-i\mathbf{k} \cdot \mathbf{R}_L) \det \tilde{\mathbf{C}}(\mathbf{k}), \quad (4)$$

where $\mathbf{R}_L = 2 \sum_{\sigma} \Delta \mathbf{r}_{\sigma} - \sum_{\beta} \Delta \mathbf{r}_{\beta}$. $\det \mathbf{C}(\mathbf{k}, \mathbf{G})$ is invariant under $p \rightarrow p + G$, where $G = |\mathbf{G}|$, and is a polynomial in $z = \exp(i2\pi p/G)$ with no negative powers of z and thus no poles. A surface zero mode exists for each zero in $\det \mathbf{C}$ with $|z| < 1$, and the Cauchy argument theorem applied to the contour $|z| = 1$ provides a count of the total number of zero modes at a particular surface:

$$\begin{aligned} n_0^S(q, \mathbf{G}) &= \frac{1}{2\pi i} \oint \frac{d \ln \det \mathbf{C}(q, z, \mathbf{G})}{dz} \\ &= -\mathbf{G} \cdot \mathbf{R}_L / (2\pi) + \tilde{n}_0^S(q, \mathbf{G}), \end{aligned} \quad (5)$$

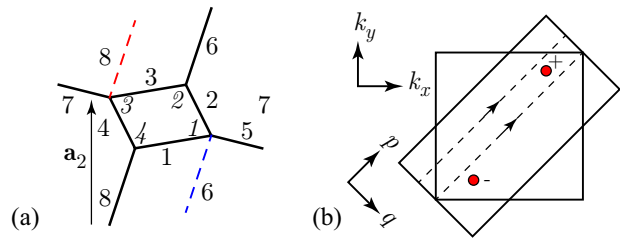


FIG. 2: (a) Different versions of the unit cell with four sites 1 – 4 labeled in italic script. The cell consisting of bonds, labeled 1 – 8 in roman script and drawn in full black, is the symmetric unit cell. A unit cell associated with a lower (an upper) surface parallel to the x -axis is constructed by moving moving bond 8 through \mathbf{a}_2 (bond 6 through $-\mathbf{a}_2$) to the dashed red (blue) line to yield $\mathbf{R}_L = -\mathbf{a}_2$ ($\mathbf{R}_L = \mathbf{a}_2$). (b) depicts the standard BZ with two Weyl points and the BZ dual to a surface-compatible unit cell oriented at 45° . The component of \mathbf{k} along the surface is q and that parallel to \mathbf{G} is p . It also shows two paths, one on each side of the projected position \mathbf{k}_w^+ the “+” Weyl point at \mathbf{k}_w^+ .

where it is understood that \mathbf{G} is the *inward* normal to the surface, $\tilde{n}_0^S(q, \mathbf{G})$ is the zero-mode count for the symmetric unit cell, whose determinant has negative powers of z , and $-\mathbf{G} \cdot \mathbf{R}_L$ is the local count of Ref. 15. In Weyl-free regions of the phase diagram, \tilde{n}_0^S reduces to the expression, $-\mathbf{G} \cdot \mathbf{R}_T / 2\pi$ derived in Ref. 15.

A Weyl point at $\mathbf{k}_w \equiv (q_w, p_w)$ is characterized by an integer winding number

$$n_w = \frac{1}{2\pi i} \oint_C d\mathbf{l} \cdot \nabla_{\mathbf{k}} \ln \det \mathbf{C} \quad (6)$$

where C is a contour enclosing \mathbf{k}_w . As a result, both $n_0^S(q, \mathbf{G})$ and $\tilde{n}_0^S(q, \mathbf{G})$ change each time q passes through the projected position of a Weyl point. Consider a lattice with a positive (+1) Weyl point at \mathbf{k}_w^+ and a negative (−1) Weyl point at $\mathbf{k}_w^- = -\mathbf{k}_w^+$, and consider a surface with an inner normal \mathbf{G} as depicted in Fig. 2(b) for $\mathbf{G} = (2\pi/a)(1, 1)$. The number of zero modes at q is calculated from a contour from $p = 0$ to $p = G$ at position q . Choose $q^{1\pm} < q_w^\pm$ and $q^{2\pm} > q_w^\pm$. Because the two paths enclose a Weyl point, the zero-mode numbers on the two sides of the Weyl point differ by the Weyl winding number

$$n_0^S(q^{2\pm}, \mathbf{G}) - n_0^S(q^{1\pm}, \mathbf{G}) = n_w = \pm 1. \quad (7)$$

Thus if $n_0^S(q < q_w^+, \mathbf{G}) = n_1^S$, the number of zero modes for $q_w^+ < q < q_w^-$ is $n_1^S + 1$, and the number for $q > q_w^-$ is again n_1^S . Fig. 3 depicts the real part κ of inverse penetration lengths of surface modes with and without Weyl points. The lengths diverge at the Weyl wavenumbers: the surface mode turns into a bulk mode that traverses the sample.

Domain walls separating two semi-infinite lattices, which we will refer to as the upper and lower lattices as in Fig. 4, with different topological and Weyl characteristics harbor topologically protected zero modes. When there are no Weyl points, the general zero-mode/SSS count is

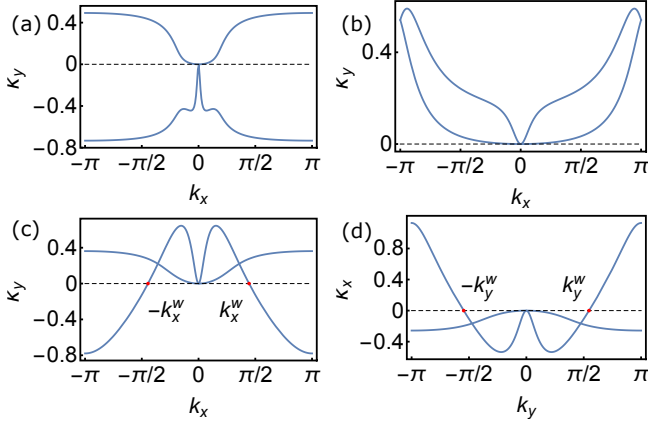


FIG. 3: Real part of inverse penetration depths for fully gapped lattices with no Weyl points [(a) with $\mathbf{R}_T = (0, 0)$ and (b) with $\mathbf{R}_T = (0, 1)$] and a lattice (c) and (d) with Weyl points. In (b), a family of zero modes has been shifted from one edge to the opposite relative to the unpolarized case (a), while in (c) and (d) the bulk zero modes are part of families split between two edges.

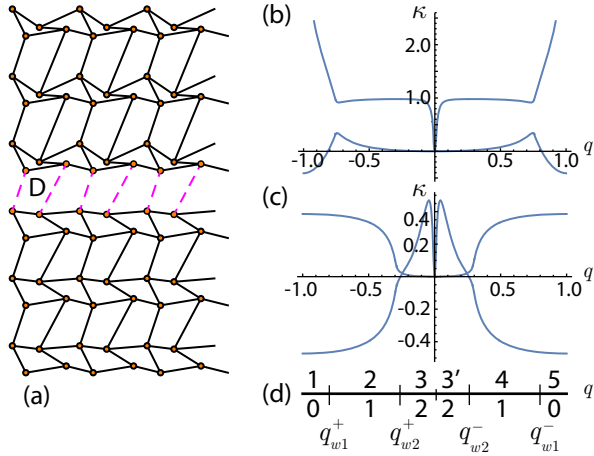


FIG. 4: (a) Two Weyl lattices with differently positioned Weyl points connected at a domain wall D. (b) and (c): the inverse penetration depths of the free surfaces of the upper and lower lattices, respectively. The upper and lower lattices have Weyl points with respective projections onto q of q_{w1}^{\pm} and q_{w2}^{\pm} with $|q_{w2}^{\pm}| > |q_{w1}^{\pm}|$. The free lower (upper) lattice has two zero modes penetrating downward (upward) for $q_{w1}^+ < q < q_{w1}^-$ ($q_{w2}^+ < q < q_{w2}^-$) and one for $|q| > |q_{w1}^+|$ ($|q| > |q_{w2}^+|$). (d) shows how the two sets of Weyl point divide the surface BZ into five regions with 0, 1, 2, 1, and 0 zero modes in the domain wall. The existence of bulk zero modes at $\mathbf{k} = 0$ divides the central region with two zero modes per q into two regions.

$\nu_S^D = n_0^D - n_S^D = -\mathbf{G} \cdot (\mathbf{R}_T^L - \mathbf{R}_T^U)/2\pi$, where n_0^D and n_S^D are, respectively, the number of zero modes and SSSs in the domain wall, \mathbf{R}_T^L and \mathbf{R}_T^U are the polarizations of the lower and upper lattices, respectively, and \mathbf{G} as in Eq. (5) is the *inward* normal (rather than the outward normal used in Ref. 15) to the top surface of the lower

lattice. When there are Weyl modes, the more general expression in terms of winding number of the symmetric unit cell [Eq. (5)] applies:

$$\nu^D(q, \mathbf{G}) = \tilde{n}_{0,L}^S(q, \mathbf{G}) + \tilde{n}_{0,U}^S(q, -\mathbf{G}). \quad (8)$$

If $\nu^D > 0$ (< 0) there are zero modes (SSSs). To prove Eq. (8) when there are no SSSs, note that the $n_{0,L}^S + n_{0,U}^S$ combined zero modes of the free surfaces of the upper and lower lattices each have independent amplitudes [see Supplementary Material]. These along with the n_B^D bond stretches per unit cell associated with the bonds required to bind the upper and lower lattices together define an $n_B^D \times (n_{0,L}^S + n_{0,U}^S)$ domain-wall compatibility matrix to which the Calladine-Maxwell index theory can be applied. When the zero-mode count of the free surfaces exceeds the number of binding bonds, the total number of zero modes in the domain wall is $n_0^D(q, \mathbf{G}) = n_{0,L}^S + n_{0,U}^S - n_B^D > 0$. When the topological (symmetric gauge) count is zero, there are no domain-wall zero modes, implying that the sum of the local counts must equal n_B^D . But the local counts depend only on surface termination and do not depend on the topological count so that $n_0^D = \tilde{n}_{0,L}^S + \tilde{n}_{0,U}^S$ is simply the topological contribution to the zero-mode count, and Eq. (8) is recovered. Direct calculation [see Supplementary Material] verifies that no SSSs are introduced when binding bonds are added. Fig. 4 shows how Weyl points in lattices connected at a domain wall divide its BZ into different regions with different numbers of zero modes.

The long-wavelength elasticity of central-force lattices is determined by the $\mathbf{k} = 0$ SSSs³². In the lattices we are considering, there are only two $\mathbf{k} = 0$ SSSs, implying that there are only two positive definite eigenvalues of the Voigt elastic matrix⁴². There are three independent strains $\boldsymbol{\varepsilon} = (\varepsilon_{xx}, \varepsilon_{yy}, \varepsilon_{xy})$, and the Voigt elastic matrix must have three positive eigenvalues and associated eigenvectors. Thus there must be one macroscopic elastic distortion that costs no energy. This is the Guest mode⁴³ that is a feature of all Maxwell lattices except those, like the kagome lattice, with extra geometry-driven states of self stress³². The elastic matrix determines the long-wavelength dynamical matrix $\mathbf{D}(\mathbf{k}) = \mathbf{Q}(\mathbf{k})\mathbf{C}(\mathbf{k})$, whose determinant is

$$\det \mathbf{D}(\mathbf{k}) \propto (\varepsilon_{yy}^G k_x^2 - 2\varepsilon_{xy}^G k_x k_y + \varepsilon_{xx}^G k_y^2)^2 \quad (9)$$

where ε_{ij}^G are the components of the strain tensor of the Guest mode. This determinant equals zero when

$$\frac{k_y}{k_x} = \frac{1}{\varepsilon_{yy}^G} \left[\varepsilon_{xy}^G \pm \sqrt{-\det(\boldsymbol{\varepsilon}^G)} \right], \quad (10)$$

where $\det(\boldsymbol{\varepsilon}^G) = \varepsilon_{xx}^G \varepsilon_{yy}^G - (\varepsilon_{xy}^G)^2$ is the determinant of the Guest strain matrix. Thus, to linear order in \mathbf{k} , there are two lines in the BZ along which there is a zero mode provided $\det(\boldsymbol{\varepsilon}^G) < 0$. These modes are either raised to finite energy by higher order terms in \mathbf{k} not described by the elastic limit; or a single Weyl mode appears along the

positive and negative parts of one of the lines. Note that this implies a quadratic rather than a linear dispersion of phonon modes near the origin and leads to inverse decay lengths that are proportional to q^2 rather than q at small a as shown in Fig. 3.

In this work, we elucidated how Weyl modes generically arise in Maxwell frames and discussed their significance using deformed square lattices as an illustration of the more general phenomenon. Indeed, in lattices with larger unit cells have additional phonon bands that more easily touch, generically leading to Weyl points and even multiple pairs thereof [see Supplementary Material]. Thus, our conclusions can be readily extended to other Maxwell lattices like origami metamaterials²⁰, ran-

dom spring networks and jammed sphere packings⁴⁴, and 3D distorted pyrochlore lattices⁴⁵ that fulfill the Maxwell condition. We also expect the presence of Weyl modes to impact the nonlinear response (e.g. buckling) in the bulk as demonstrated for edge modes^{17,18}.

We are grateful to Charles Kane for many informative discussions and suggestions. (DZR) thanks NWO and the Delta Institute of Theoretical Physics for supporting his stay at the Institute Lorentz. MJF was supported by the Department of Defense (DoD) through the National Defense Science & Engineering Graduate Fellowship (NDSEG) Program. This work was supported in part by DMR-1104707 and DMR-1120901 (TCL), as well as FOM and NWO (BGC, VV).

-
- * Current address: Department of Physics, University of Massachusetts, Amherst, MA 01002, USA
- ¹ N. Nakamura, *Geometry, Topology and Physics* (Institute of Physics Publishing, Bristol, 2008), 2nd ed., p. 79 and chapter 12.
 - ² G. E. Volovik, *The Universe in a Helium Droplet* (Clarendon, Oxford, 2003).
 - ³ G. Volovik, *Lecture Notes in Physics* **718**, 3173 (2007).
 - ⁴ W. P. Su, J. R. Schrieffer, and A. J. Heeger, *Phys. Rev. Lett.* **42**, 1698 (1979).
 - ⁵ R. Jackiw and C. Rebbi, *Phys. Rev. D* **13**, 3398 (1976).
 - ⁶ B. I. Halperin, *Phys. Rev. B* **25**, 2185 (1982), ISSN 0163-1829.
 - ⁷ F. D. M. Haldane, *Phys. Rev. Lett.* **61**, 2015 (1988), ISSN 0031-9007.
 - ⁸ C. L. Kane and E. J. Mele, *Phys. Rev. Lett.* **95**, 146802 (2005), ISSN 0031-9007.
 - ⁹ B. A. Bernevig, T. L. Hughes, and S.-C. Zhang, *Science* **314**, 1757 (2006).
 - ¹⁰ J. E. Moore and L. Balents, *Phys. Rev. B* **75**, 121306 (2007).
 - ¹¹ L. Fu, C. L. Kane, and E. J. Mele, *Phys. Rev. Lett.* **98**, 106803 (2007).
 - ¹² Z. Hasan and C. Kane, *Rev. Mod. Phys.* **82**, 3045 (2010).
 - ¹³ X.-L. Qi and S.-C. Zhang, *Rev. Mod. Phys.* **83**, 1057 (2011).
 - ¹⁴ E. Prodan and C. Prodan, *Phys. Rev. Lett.* **103**, 248101 (2009).
 - ¹⁵ C. Kane and T. C. Lubensky, *Nature Phys.* **10**, 39 (2014).
 - ¹⁶ J. Paulose, B. G. Chen, and V. Vitelli, *Nature Physics* **11**, 153 (2015), ISSN 1745-2473.
 - ¹⁷ J. Paulose, A. S. Meeussen, and V. Vitelli, *Proceedings of the National Academy of Sciences of the United States of America* **112**, 7639 (2015), ISSN 0027-8424.
 - ¹⁸ B. G. Chen, N. Upadhyaya, and V. Vitelli, *Proceedings of the National Academy of Sciences of the United States of America* **111**, 13004 (2014), ISSN 0027-8424.
 - ¹⁹ V. Vitelli, N. Upadhyaya, and B. G. Chen, arXiv:1407.2890 (2014).
 - ²⁰ B. G. Chen, B. Liu, A. A. Evans, J. Paulose, I. Cohen, V. Vitelli, and C. D. Santangelo, arXiv (2015).
 - ²¹ M. Xiao, G. Ma, Z. Yang, P. Sheng, Z. Q. Zhang, and C. T. Chan, *Nature Physics* **11** (2015).
 - ²² H. C. Po, Y. Bahri, and A. Vishwanath (2014), 1410.1320.
 - ²³ Z. Yang, F. Gao, X. Shi, X. Lin, Z. Gao, Y. Chong, and B. Zhang, *Physical Review Letters* **114**, 1 (2015).
 - ²⁴ L. M. Nash, D. Kleckner, V. Vitelli, A. M. Turner, and W. T. M. Irvine, arXiv (2015), 1504.03362v1.
 - ²⁵ P. Wang, L. Lu, and K. Bertoldi, arXiv (2015), 1504.01374v1.
 - ²⁶ Y.-T. Wang, P.-G. Luan, and S. Zhang, *New Journal of Physics* **17**, 073031 (2015).
 - ²⁷ R. Susstrunk and S. D. Huber, *Science* **349**, 47 (2015), 1503.06808v1.
 - ²⁸ T. Kariyado and Y. Hatsugai, arXiv:1505.06679 (2015).
 - ²⁹ V. Peano, C. Brendel, M. Schmidt, and F. Marquardt, *Phys. Rev. X* **5**, 031011 (2015).
 - ³⁰ S. H. Mousavi, A. B. Khanikaev, and Z. Wang, arXiv:1507.03002 (2015).
 - ³¹ A. B. Khanikaev, R. Fleury, S. H. Mousavi, and A. Al, *Nat. Comm.* **6** (2015).
 - ³² T. C. Lubensky, C. L. Kane, X. Mao, A. Souslov, and K. Sun, *Reports on progress in physics. Physical Society (Great Britain)* **78**, 073901 (2015).
 - ³³ X. G. Wan, A. M. Turner, A. Vishwanath, and S. Y. Savrasov, *Physical Review B* **83**, 205101 (2011), ISSN 1098-0121.
 - ³⁴ A. A. Burkov and L. Balents, *Physical Review Letters* **107**, 127205 (2011), ISSN 0031-9007.
 - ³⁵ A. A. Burkov, M. D. Hook, and L. Balents, *Physical Review B* **84**, 235126 (2011), ISSN 1098-0121, burkov, A. A. Hook, M. D. Balents, Leon.
 - ³⁶ J. P. Liu and D. Vanderbilt, *Physical Review B* **90**, 155316 (2014), ISSN 1098-0121.
 - ³⁷ S.-Y. Xu, I. Belopolski, A. Nasser, M. Neupane, G. Bian, C. Zhang, R. Sankar, G. Chang, Z. Yuan, C.-C. Lee, et al., *Science* **249**, 613 (2015).
 - ³⁸ L. Lu, L. Fu, J. D. Joannopoulos, and M. Soljacic, *Nature Photonics* **7**, 294 (2013), ISSN 1749-4885.
 - ³⁹ L. Lu, Z. Wang, D. Ye, L. Rain, J. D. Joannopoulos, and M. Soljacic, arXiv:1502.03438v1 (2015).
 - ⁴⁰ K. Sun, A. Souslov, X. Mao, and T. C. Lubensky, *PNAS* **109**, 12369 (2012).
 - ⁴¹ C. R. Calladine, *Int. J. Solids Struct.* **14**, 161 (1978).
 - ⁴² N. W. Ashcroft and N. D. Mermin, *Solid State Physics* (Cenage Learning, New York, 1976), 1st ed.
 - ⁴³ S. D. Guest and J. W. Hutchinson, *J. Mech. Phys. Solids* **51**, 383 (2003), ISSN 0022-5096.

⁴⁴ D. M. Sussman, O. Stenull, and T. C. Lubensky, unpublished (2015).

⁴⁵ O. Stenull, C. L. Kane, and T. C. Lubensky, unpublished (2015).

Supplementary Material

Topological polarization via winding number

In this section, we calculate the topological polarization of lattices with and without Weyl modes. We consider lattices with particles lying at sites $\mathbf{b}_i + \mathbf{R}$, where $\{\mathbf{b}_i\}$ are the basis vectors giving the site positions within a unit cell and $\mathbf{R} \equiv n_1\mathbf{l}_1 + n_2\mathbf{l}_2$ is the position of the cell, with $\mathbf{l}_1, \mathbf{l}_2$ the Bravais vectors. A phonon mode may be expressed as $\mathbf{u}(\mathbf{R}) = \exp(i\mathbf{k} \cdot \mathbf{R}) \mathbf{u}$, where \mathbf{u} is a vector of displacements within a crystal cell. More generally, we can locally satisfy the dynamics with modes that exponentially grow and decay as well as oscillating, taking the form:

$$\mathbf{u}(\mathbf{R}) = \exp[(i\mathbf{k} - \boldsymbol{\kappa}) \cdot \mathbf{R}] \mathbf{u} \equiv z_1^{n_1} z_2^{n_2} \mathbf{u}, \quad (11)$$

where the components of $\boldsymbol{\kappa}$ describe the mode's growth and decay and are plotted in Fig. 3 of the main text. Note that z_1, z_2 are given by

$$\begin{aligned} z_1 &= \exp[(i\mathbf{k} - \boldsymbol{\kappa}) \cdot \mathbf{l}_1], \\ z_2 &= \exp[(i\mathbf{k} - \boldsymbol{\kappa}) \cdot \mathbf{l}_2]. \end{aligned} \quad (12)$$

If $\boldsymbol{\kappa} = 0$, the complex numbers z_1, z_2 have unit magnitude and represent a purely oscillatory phonon mode in the bulk.

For a deformed square lattice (choosing a symmetric unit cell) the four intercellular bonds then generate terms in the compatibility matrix proportionate to $z_1, z_2, z_1^{-1}, z_2^{-1}$ so that for fixed z_2 the determinant has the form

$$\det(\mathbf{C}(z_1, z_2)) \sim b_{-1}(z_2)z_1^{-1} + b_0(z_2) + b_1(z_2)z_1, \quad (13)$$

where the $\{b_i\}$ are complex functions of z_2 . From this, we could solve for the two exact values of z_1 where the determinant vanishes, signaling the presence of a zero mode. Of particular significance is whether $|z_1|$ is greater than one, indicating a zero mode on the right edge of the system, or less than one, indicating a zero mode on the left edge. This can be determined entirely in terms of the winding of the bulk modes around the Brillouin zone, those in which z_1 has the form $\exp(ik_x)$, for a winding number

$$\begin{aligned} & \frac{1}{2\pi} \int_0^{2\pi} dk_x \ln \frac{\partial}{\partial k_x} \det[\mathbf{C}(\exp(ik_x), \exp(ik_y))] \\ &= \frac{1}{2\pi} \oint_C dz_1 \frac{\frac{\partial}{\partial z_1} \det(\mathbf{C}(z_1, \exp(ik_y)))}{\det(\mathbf{C}(z_1, \exp(ik_y)))}. \end{aligned} \quad (14)$$

Because $k_x = 0$ and $k_x = 2\pi$ correspond to the same point in the Brillouin zone, the real parts of these integrals vanish and the imaginary part is the change in phase of $\det(z_1, \exp(ik_y))$ as one follows the contour C around the unit circle. According to the Argument Principle, obtained via performing a contour integral, this integral is $2\pi i(N - P)$, where N and P are respectively the number of zeroes and poles of $\det(z_1, \exp(ik_y))$ enclosed by the contour. Thus, windings of $-2\pi, 0$, and 2π correspond respectively to 0, 1 and 2 zeroes of $\det(z_1, \exp(ik_y))$ lying in the unit circle and consequently 0, 1 or 2 zero modes on the left edge of the system, with the remaining 2, 1, or 0 lying on the right.

To obtain all the zero modes we must repeat this winding calculation for all values of k_y , but for lattices without Weyl modes this proves trivial—the path may be continuously deformed across the Brillouin zone (the zero at the origin has zero winding number and so is trivial) and so we find that none, half, or all of the horizontal zero modes lie on the left wall of the system. Similarly, calculating the winding of $\det(\exp(ik_x), \exp(ik_y))$ as k_y advances by 2π determines how many zero modes lie on the top and bottom edges of the system. Combining these two values into a vector gives us the *topological polarization* of a lattice, which points in the average direction of zero modes:

$$\mathbf{R}_T = \frac{-1}{2\pi} (\Delta\phi(\mathbf{k} \rightarrow \mathbf{k} + 2\pi(1, 0)), \Delta\phi(\mathbf{k} \rightarrow \mathbf{k} + 2\pi(0, 1))). \quad (15)$$

This topological polarization is uniquely defined and independent of \mathbf{k} provided that there are no Weyl modes. \mathbf{R}_T , along with the local vector \mathbf{R}_L , determines the number of zero modes on a surface specified by a reciprocal lattice vector \mathbf{G} as discussed in Eq. (5). Consider, as a simple example, an $L \times L$ lattice where the open boundary is made up of straight cuts along reciprocal lattice vectors that do not split any cells. For such a lattice with topological polarization $(0, 0)$ there are L zero modes on each edge, while a lattice with topological polarization $(0, 1)$ has $2L$ modes on its top edge and none on its bottom edge.

Winding of the phase across the Brillouin zone and about a Weyl point

As discussed in the previous section, the winding of the phase of $\det \mathbf{C}(\mathbf{k})$ through the Brillouin zone determines both the presence of Weyl modes and the topological polarization of the lattice. Consider the path shown in Fig. 5. We consider only noncritical lattices, so that the determinant vanishes only at $\mathbf{k} = (0, 0)$ and possibly at a pair of Weyl points located at $\pm \mathbf{k}_W$. The path chosen thus has a well-defined phase and encloses at most one Weyl point. A winding of ± 1 indicates the presence of a Weyl point, while a winding of 0 indicates a lattice without finite-wavenumber zero modes.

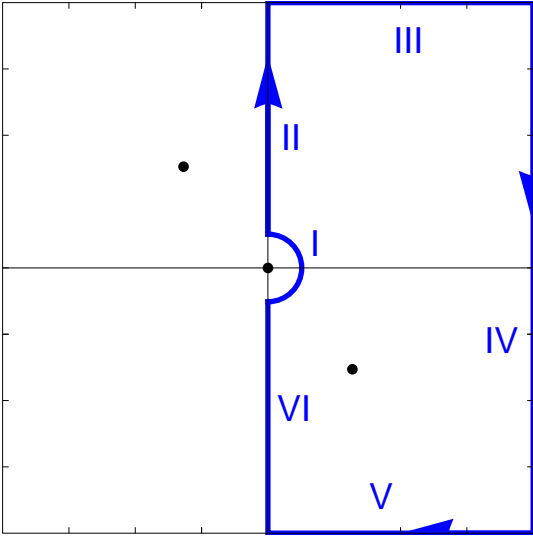


FIG. 5: The path around the Brillouin zone along which the winding is evaluated. A winding of +1 or -1 indicates the presence of a Weyl point (shown as a black dot), while a winding of 0 indicates that the lattice has no Weyl modes. The indentation along path I avoids the zero modes at $\mathbf{k} = 0$. When no Weyl points are present, the winding along the path VI, I, II yields one component of the topological polarization, with the other component being given by a similar horizontal path, as described in the main text.

Consider first the segments II and VI. From the form of the determinant, which must have a double root at $z_1 = z_2 = 1$ corresponding to the two translational modes, it may be shown that along either of these segments the determinant is real and nonzero, so its winding does not change.

Note that \mathbf{C} is periodic under $\mathbf{k} \rightarrow \mathbf{k} + 2\pi(0, 1)$. Thus, while the winding along segment III may be finite, it must be canceled by the return path along segment V. Thus, the winding comes entirely from segment I (the “origin term”) and segment IV (the “edge term”).

Along segment IV, $k_x = \pi$ and

$$\det \mathbf{C}(\mathbf{k}) \sim a \exp(ik_y) + b + c \exp(-ik_y), \quad (16)$$

where (a, b, c) are real lattice-dependent numbers. As k_y goes from π to $-\pi$, $\det \mathbf{C}(\mathbf{k})$ travels along an elliptical path that may be either clockwise or counterclockwise and may or may not enclose the origin, leading to a winding

$$\begin{aligned} \text{winding}(IV) &= \text{Sign}(c - a) \\ &\times [\text{Sign}(a + b + c) - \text{Sign}(b - a - c)]/2. \end{aligned} \quad (17)$$

Along segment I, $\det \mathbf{C}(\mathbf{k})$ takes its long-wavelength form

$$\begin{aligned} \det \mathbf{C}(\mathbf{k}) &\sim ak_y^2 + bk_xk_y + ck_x^2 + \\ &i(dk_xk_y^2 + ek_x^2k_y) + O(|\mathbf{k}|^4), \end{aligned} \quad (18)$$

where these lattice-dependent real parameters (a, b, c, d, e) differ from those of Eq. (16). In the neighborhood of the origin, the determinant has a real part $O(|\mathbf{k}|^2)$ and an imaginary part $O(|\mathbf{k}|^3)$. Thus, its phase can only appreciably change when the real part passes through zero, along lines

$$k_y = \alpha_{\pm} k_x; \quad \alpha_{\pm} = \left(-b \pm \sqrt{b^2 - 4ac}\right)/(2a). \quad (19)$$

If the discriminant is negative, segment I does not pass through any such lines, and so the determinant does not undergo any sort of winding. Otherwise, it passes by the origin twice, with imaginary parts

$$v_1 = (d\alpha_1 + e\alpha_1^2) |\mathbf{k}|^3, \quad (20)$$

$$v_2 = (d\alpha_2 + e\alpha_2^2) |\mathbf{k}|^3, \quad (21)$$

where α_1 is $\text{Min}(\alpha_{\pm})$, so the segment passes through $k_y = \alpha_1 k_x$ first. Clearly, segment I begins and ends near ak_y^2 and undergoes finite winding only when v_1 and v_2 differ in sign. The winding is

$$\text{winding}(I) = \text{Sign}(a) [\text{Sign}(v_1) - \text{Sign}(v_2)]/2. \quad (22)$$

Thus, the sum of the origin term and the edge term gives the winding around half of the Brillouin zone, which indicates the presence or absence of Weyl modes in the lattice. In the absence of such Weyl modes, the winding along segments VI, I and II (of which only the second is nonzero) is the winding along any path that increases by $(0, 2\pi)$. This is one component of the topological polarization. The other component is readily obtained by repeating the analysis along a similarly-indented path from $(-\pi, 0)$ to $(\pi, 0)$. Thus, the same analysis of winding numbers that identifies lattices with Weyl modes determines the topological polarizations of those without such modes.

For lattices with larger unit cells, the calculation becomes more complicated. Each intercellular bond introduces an additional factor of z_1, z_2, z_1^{-1} or z_2^{-1} into $\det \mathbf{C}$, increasing the polynomial degree. Weyl points are zeroes of this expression satisfying $|z_1| = |z_2| = 1$. Hence, in larger unit cells allow more solutions of these equations and hence more Weyl points, or even multiple pairs of Weyl points.

Domain-wall zero modes: count and structure

As discussed in the text following Eq. (8), the number of zero modes and their structure can be obtained from

the eigenvalues for z and the associated eigenvectors of the zero modes of the free surfaces of the upper and lower lattices that are joined together at the wall. Here we outline the derivation of this result. The upper and lower lattices have, respectively, $n_{0,U}^S$ and $n_{0,L}^S$ zero surface modes at their free surfaces. Let the z -eigenvalues and associated eigenvectors for zero modes of the upper and lower lattices at given q along the wall be $z_{\mu+}(q)$, $(\mathbf{a}_1^{\mu+}, \mathbf{a}_2^{\mu+}, \mathbf{a}_2^{\mu+}, \mathbf{a}_2^{\mu+})$ and $z_{\mu-}(q)$, $(\mathbf{a}_1^{\mu-}, \mathbf{a}_2^{\mu-}, \mathbf{a}_2^{\mu-}, \mathbf{a}_2^{\mu-})$, respectively, where $\mathbf{a}_n^{\mu\pm}$ is the displacement of site n in the unit cell and by definition $\mathbf{C}_{\pm}(q, z_{\mu\pm}, G)\mathbf{a}_{\mu\pm} = 0$ where \mathbf{C}_{\pm} is the compatibility matrix of the upper (+) or lower (-) lattice. Any linear combination of zero modes,

$$\mathbf{u}_n^{\pm}(q, n_x, n_y) = \sum_{\mu\pm} A^{\mu\pm} \mathbf{a}_n^{\mu\pm} (z_{\mu\pm}(q))_y^n e^{in_x q} \quad (23)$$

is also a zero mode, where n_x and n_y are the positions of unit cell along x and y . Denote the n_B^D unit vectors along the bonds that bind the upper and lower lattices by \mathbf{b}_{α} . Each bond α connects an upper lattice boundary site $n_+(\alpha)$ to a lower lattice site $n_-(\alpha)$. The lengths of these binding bonds must not change in a domain-wall zero mode. If we restrict displacements of the upper and lower lattices to their surface modes, the length of no bond will change provided, the binding bonds satisfy

$$\mathbf{b}_{\alpha} \cdot [\mathbf{u}_{n_+(\alpha)}^+(q, n_x, 0) - \mathbf{u}_{n_-(\alpha)}^-(q, n_x, 0)] = 0 \quad (24)$$

for all α and any zero-mode displacements $\mathbf{u}_{n_{\pm}(\alpha)}^{\pm}(q, n_x, 0)$ of the upper and lower lattices. Then,

Eqs. (23) and (24) can be written as $\mathbf{C}^D \cdot \mathbf{A} = 0$, where \mathbf{A} with components $A^{\mu\sigma}$, $\sigma = \pm$, is the $(n_{0,U}^S + n_{0,L}^S)$ -dimensional column vector of displacement amplitudes and the components of the $n_B^D \times (n_{0,U}^S + n_{0,L}^S)$ domain-wall compatibility matrix are

$$C_{\alpha, \mu\sigma}^D = \sigma \mathbf{b}_{\alpha} \cdot \mathbf{a}_{n_{\sigma}(\alpha)}^{\mu\sigma}. \quad (25)$$

The null space of this matrix is the space of zero modes of the domain wall.

As a specific example, consider the lattice shown in Fig. 6 (a) with a domain wall connecting a lattice with its inverted image. The real parts of the inverse decay lengths of these two lattices are the same and are depicted in Fig. 7. For $q > 1$, there are two positive decay lengths yielding $n_{0,2}^S = n_{0,U}^S = 2$. Two bonds per unit cell connect the two lattices, so $n_B^D = 2$ and \mathbf{C}^D is a 2×4 dimensional matrix

$$\mathbf{C}^D = \begin{pmatrix} \mathbf{b}_1 \cdot \mathbf{a}_4^{1+} & \mathbf{b}_1 \cdot \mathbf{a}_4^{2+} & -\mathbf{b}_1 \cdot \mathbf{a}_3^{1-} & -\mathbf{b}_1 \cdot \mathbf{a}_3^{2-} \\ \mathbf{b}_2 \cdot \mathbf{a}_1^{1+} & \mathbf{b}_2 \cdot \mathbf{a}_1^{2+} & -\mathbf{b}_2 \cdot \mathbf{a}_2^{1-} & -\mathbf{b}_2 \cdot \mathbf{a}_2^{2-} \end{pmatrix} \quad (26)$$

As expected, this matrix has a two-dimensional null space, and there are two zero domain-wall zero modes. Their wave functions for $q = 2.0$ are depicted in Fig. 6 (b) and (c).

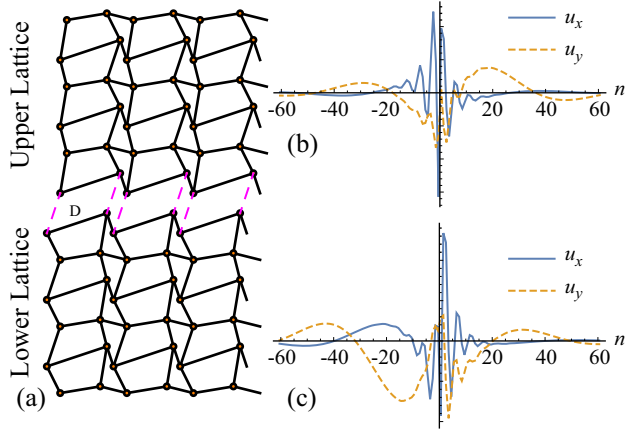


FIG. 6: (a) A lattice with a domain wall connecting a lower lattice to an upper lattice, which is a 180 degree rotation of the lower lattice. (b) and (c) Spatial representations of the displacement of site 1 of the upper lattice (positive cell index n) and site 2 of the lower lattice (negative n) (following the naming convention of Fig. 2) for the two zero modes at $q = 2.0$.

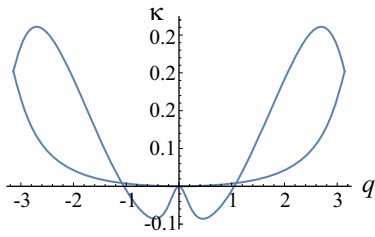


FIG. 7: The real part of the inverse penetration depth κ as a function of wavenumber q for a surface parallel to the x -axis. A positive value of κ implies a decaying solution into the bulk. Thus, there are two decaying solutions for $q = 2.0$.